Proceedings of the 10th International Pipeline Conference
IPC2014
September 29-October 3, 2014, Calgary, Alberta, Canada

IPC2014-33582

EVALUATION OF PRESSURIZED COLD BEND PIPE BODY TENSILE FRACTURES UNDER BENDING LOADS

Celal Cakiroglu
Department of Civil and Environmental Engineering, University of Alberta
Edmonton, Alberta, Canada

Muntaseer Kainat
Department of Civil and Environmental Engineering, University of Alberta
Edmonton, Alberta, Canada

Samer Adeeb
Department of Civil and Environmental Engineering, University of Alberta
Edmonton, Alberta, Canada

J. J. Roger Cheng
Department of Civil and Environmental Engineering, University of Alberta
Edmonton, Alberta, Canada

Millan Sen
Enbridge Pipelines Inc.
Edmonton, Alberta, Canada

ABSTRACT

Cold bending is applied at locations where the pipeline direction has to be changed in a horizontal or vertical plane. The process of cold bending usually results in residual stresses as well as changes in the material properties at the vicinity of the cold bend location which makes the study of the mechanical behaviour of cold bends indispensable. Due to discontinuous permafrost in arctic regions as well as slope instabilities and earthquakes cold bends within pipelines constructed in such locations can be subjected to significant tensile or compressive forces.

Experimental studies were carried out by Sen et al [1][2][3]in order to investigate the buckling behaviour of pressurized cold bends. In these experiments the curvature of the cold bend is increased in the presence of a constant internal pressure. In their experimental study a total of 8 full scale tests were conducted with a variety of pipe diameters, diameter to wall thickness ratio and steel grade. In this set of full scale tests one of the pipes with grade X65 failed due to fracture at the extrados after buckling and formation of wrinkles at the intrados[1].

Our previous work [4], [5] on this subject showed the simulations of this case using finite element analysis. These simulations demonstrated that indeed pipe body tensile side fracture can be observed for this particular pipe specification. Whereby the tension side fractures are expected starting from a specific internal pressure level. The simulation results showed that the equivalent plastic strain values at the cold bend extrados increase dramatically starting from a certain level of applied curvature in load cases with an internal pressure higher than a transition value. In this paper the effect of steel grade on this transition from compressive to tensile failure is investigated. Parametric studies are conducted for the entire range of steel grades tested in the experimental study of Sen et al. It is found that there is a linear proportionality between the steel grade and the transition internal pressure for steel grades between X60 and X80.

NOMENCLATURE

PEEQ	Equivalent plastic strain
SMYS	Specified minimum yield stress [MPa]
κ	Curvature of the cold bend [1/mm]
θ	Bend angle
R_0	Initial radius of curvature of the cold bend
R	Current radius of curvature of the cold bend
H_0	Initial horizontal length of the cold bend
L	Total length of the cold bend
u	Displacement of the loading pin [mm]
Intrados	Compression side of the cold bend
Extrados	Tension side of the cold bend
t	Pipe wall thickness [mm]
OD	Outer diameter of the pipe [mm]
E	Modulus of elasticity

1 INTRODUCTION

Pipelines can undergo significant amounts of tension and bending moments due to landslides, seismic activities as well as discontinuous permafrost. Also excessive temperature gradients between the installation and operating temperatures affect the material behaviour of pipes considerably. Due to these mechanical effects on the pipe structure it is important to have a thorough understanding of pipeline structural response under applied forces.

Cold bending is a procedure which changes the pipeline direction in a horizontal or vertical plane in order to make the pipeline direction conform to the terrain conditions. In the process of cold bending residual stresses are concentrated in the vicinity of the cold bent part. The plastic material response is also affected in this process since the extrados of the cold bend is loaded beyond the yield stress in tension and the intrados of the cold bend is loaded beyond the yield stress in compression. Experimental studies carried out by Caminada et al [6] on cold bends with an R/OD ratio of 4.5 and grade T92 showed a 22% increase of the yield strength at the extrados and 18% decrease of the yield strength at the intrados. This experimental outcome also confirms that failure at the compression side is more likely to occur in cold bended pipes due to the decreased mechanical properties at the intrados in the cold bending process. Moreover, the deformations caused by soil-pipe interaction tend to accumulate at the cold bent parts. As cold bends have a lower stiffness than straight pipes, and thus such deformations are expected to be concentrated at cold bends [7]. All these conditions make the cold bends especially prone to buckling and rupture under bending loads.

Sen et al, [1], [2], [3] conducted comprehensive experimental research in order to analyze the structural response of cold bended pipes under internal pressure and in-plane bending. In this research project a total of 8 full scale specimens with steel grades X60, X65 and X80 were tested. In one of the full scale tests of this research project an X65 cold bent pipe under in-plane bending load and 80% SMYS internal pressure ruptured at the tension side in an unexpected way after the formation of wrinkles at the compression side (Figure 1). This rare mode of failure is usually not considered in the design of cold bends since tensile failure is considered to be a type of structural failure associated with girth weld locations. The experimental setup for this particular test is shown in Figure 2. The schematic in Figure 2 shows that the sections of the pipe wall adjacent to the end plates are covered with collars in order to prevent these sections from buckling. This prevention is necessary in order to eliminate the effect of the end plates on the structure and to have an experimental setup which resembles the field conditions. In the setup of Figure 2 the displacement load is applied on the pipe on one side using a bending beam which is connected to the moment arm with a hinge. This connection point is referred to as the **loading pin** in the subsequent parts of this paper. The position of the other end plate is kept fixed throughout the test.

In our previous work [4], [5] this particular cold bend configuration is simulated both with and without internal pressure using the finite element simulation software Abaqus version 6.12. The material properties and geometry used in these simulations of the X65 cold bend are given in Table 1.

In these simulations it was found that the presence of internal pressure has a decisive effect on the failure mode of the structure. In the absence of internal pressure a diamond shaped wrinkle was observed on the compression side of the cold bend and material plastification was concentrated around this wrinkle location (Figure 3). On the other hand in the case of loading with internal pressure corresponding to 80% SMYS hoop stress the highest equivalent plastic strain values were observed at the tension side of the cold bend. These high plastic strains were observed after the formation of an outward wrinkle at the compression side of the cold bend (Figure 4).

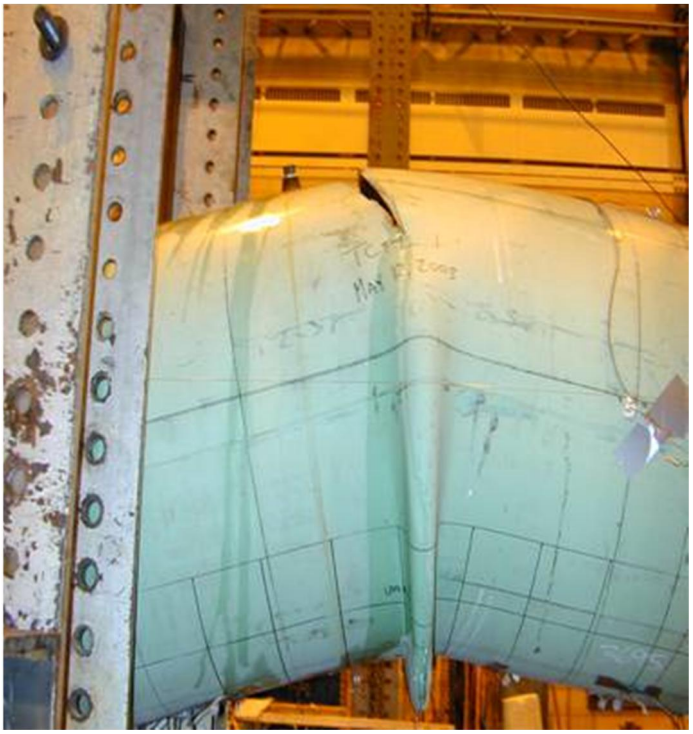

Figure 1: Wrinkle and Fracture of the Test Specimen [1]

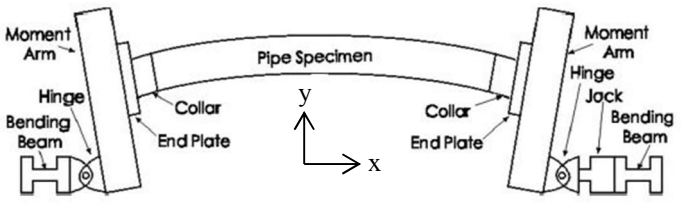

Figure 2: Experimental setup [2]

Table 1: Geometric and mechanical properties of the X65 cold bend

Modulus of Elasticity [MPa]	201530
SMYS [MPa]	448
Ultimate strength [MPa]	531
Pipe outer diameter (OD) [mm]	762
Thickness of collar reinforced sections [mm]	16
Length of the collar reinforced sections [mm]	237
Diameter to wall thickness ratio	93
Initial radius of curvature [mm]	17796
Initial curvature [1/mm]	$5.62 \cdot 10^{-5}$
Pipe total length [mm]	7454
Pipe horizontal length [mm]	7400

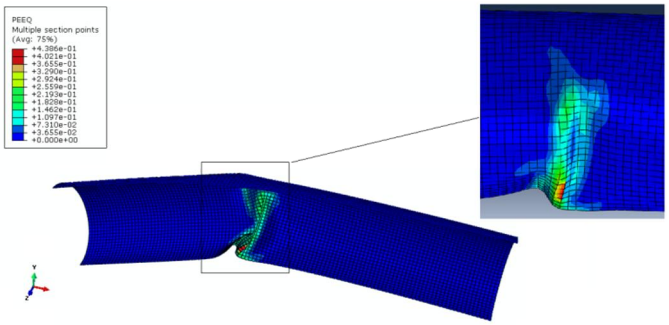

Figure 3: Plastic strain distribution under bending load without internal pressure [4]

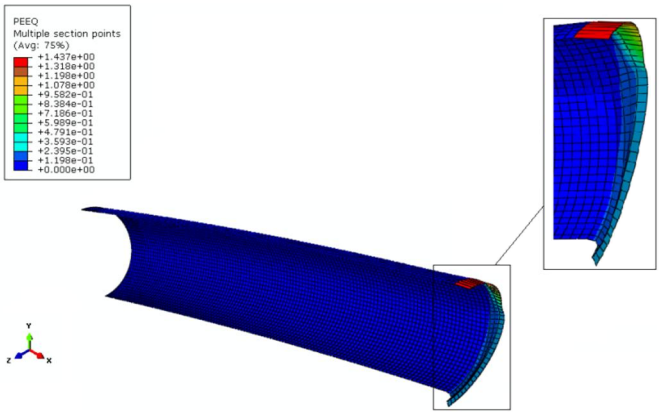

Figure 4: Plastic strain distribution under bending load and internal pressure [4]

In order to better understand the effect of internal pressure on the failure mode, a parameteric study is conducted in [5]. In this parametric study the internal pressure is varied between 20% SMYS and 80% SMYS hoop stress. The same X65 specimen is simulated under 10 different internal pressure values in this range. The results of this parametric study showed that at an internal pressure which corresponds to 67% SMYS hoop stress, the failures mode changes from compression side failure to tension side failure. In this current work, the objective is to gain a more precise value of the transition pressure for X65 as well as the other steel grades tested in the experiments of Sen et al. In order to have a unified criterion for the material failure, the amount of equivalent plastic strain variable is utilized. An equivalent plastic strain level of 40% is designated to be the indication of material failure.

In this paper, in addition to the internal pressure also the effect of steel grade on the failure mode is investigated. Parametric studies are carried out for cold bends with steel grades X60, X65 and X80. It was found that a linear proportionality exists between the level of internal pressure at the transition from compressive to tensile failure and the steel grade.

2 METHODS OF NUMERICAL MODELLING

The finite element analysis software Abaqus is utilized in order to simulate the structural response of cold bends having the geometric dimensions listed in Table 1. In all simulations the pipe geometry is meshed using 4-node general purpose shell elements with reduced integration (S4R). A non-linear isotropic hardening material behaviour is adopted in order to model the plastic material response. In this model, the relationship between the yield stress and the plastic strain is assumed to be non-linear between the initial yield stress and the ultimate strength,. 237 mm long sections of the pipe next to the end plates are assigned a greater element thickness (16 mm) than the rest of the model (8.2 mm) in order to model the effect of the reinforcing collars (Figure 2) and to prevent an inappropriate buckling of the model due to the pipe - end plate interaction. The moment arm (Figure 2) is modeled using rigid beam and multi point constraints. The nodes on the left pipe edge (Figure 3, Figure 4) are connected to a reference point at the centroid of the cross section of the pipe edge using multi-point constraints. This reference point, on the other hand, is connected to another reference point 600 mm below in y-direction with rigid beam constraints. This reference point located 600 mm below the pipe axis represents the loading pin.

In order to increase the computational efficiency of the model, symmetry conditions are introduced. For this purpose symmetry planes parallel to x-y and y-z planes are introduced and one quarter of the entire cold bend pipe is simulated. Besides reducing the computation time, introducing symmetry boundary conditions also brings the advantage of excluding the out - of - plane buckling modes from the simulations. This makes the simulations more realistic since the out-of-plane displacement of the specimen was also constrained in the experimental setup.

As the first step of the simulations, internal pressure is applied on the inner surfaces of the pipe wall. In the parametric studies of the effect of internal pressure, the pressure value is

varied between 1.93 MPa and 7.72 MPa which correspond to 20% SMYS and 80% SMYS hoop stress respectively. In the next step of the simulations a displacement load of 298.99 mm is applied to the loading pin in x-direction causing the closing mode bending stresses and increasing the initial curvature of the cold bend.

2.1 MATERIAL MODEL

The non-linear stress/strain response in the plastic regime of the pipe base metal is adopted according to the Ramberg - Osgood model as per CSA Z662-11 (Clause C.5.7.1.3)[8]. The SMYS and the Ultimate Strengths of the different grades of steel are selected according to the API 5L specifications (Table 2).

Table 2: Material Specifications according to API 5L

Grade	SMYS		Tensile Strength	
	Ksi	Mpa	Ksi	Mpa
X 60	60	415	75	520
X 65	65	450	77	530
X 80	80	555	90	625

From the true stress and strain values, appropriate yield stress and equivalent plastic strain values are calculated and input into the FEA model. The material models are first tested on a single plane stress shell element, and are accepted upon observing good agreement between the FEA response and the original Ramberg-Osgood model.

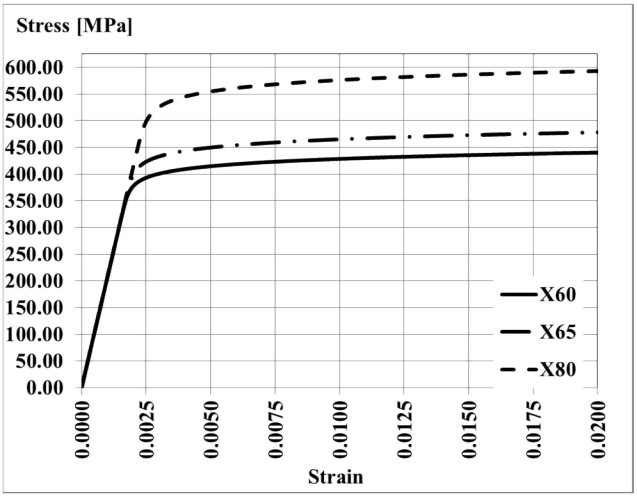

Figure 5: Ramberg - Osgood material model for X60, X65 and X80

2.2 MODELLING THE PIPE CURVATURE

In the current work the variable of applied displacement is replaced with the cold bend curvature in the visualization of all parameters which show a variation with respect to displacement. The motivation for that is to generalize the reaction force and equivalent plastic strain variations obtained for a particular pipe geometry to all possible geometric configurations.

The curvature of the cold bend is calculated based on the assumption that as the displacement of the loading pin (u) is applied, the cold bend deforms into a circular arc with a radius of curvature (R). Although in practice cold field bends do not have perfect curvature because of being progressively kinked, this assumption allows us to approximate the overall curvature of the cold bend. The nonlinear relationship between u and R is a function of the total length of the cold bend (L), the bend angle ($\theta = \frac{L}{2R}$) and the initial horizontal length of the cold bend (H_0) as follows:

$$2 \cdot R \cdot \sin\left(\frac{L}{2R}\right) = H_0 - u \quad (1)$$

As the curvature of the cold bend ($\kappa = \frac{1}{R}$) is a better measure for the cold bend deformation, for each applied u, the corresponding R was obtained by numerically solving the above equation. For the derivation of the expression for κ the reader is referred to [9]. The numerical algorithm makes use of the fact that the initial radius of curvature R_0 is known and that increasing u decreases R (Figure 6). The nonlinear relationship between the applied displacement u and the curvature of the pipe κ is illustrated in Figure 7. In the rest of this paper, for each displacement of the loading pin the corresponding curvature value is used as a measure of deformation since the usage of the applied displacement would make the results of this study limited to a specific geometric configuration.

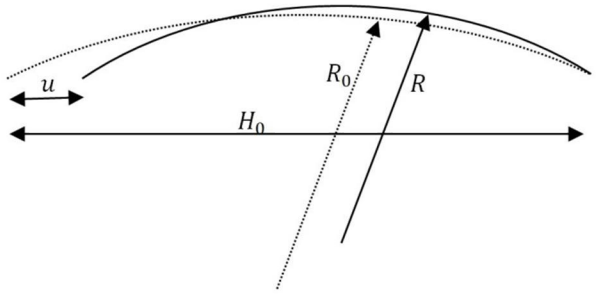

Figure 6: Initial and deformed configurations of the cold bend axis

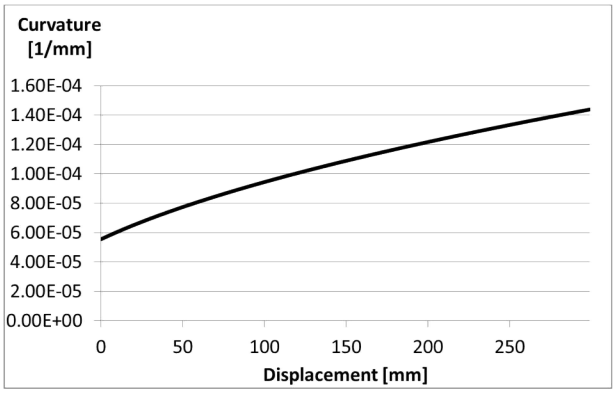

Figure 7: Variation of the curvature with respect to applied displacement

3 RESULTS OF THE PARAMETRIC STUDIES

In this section the parametric studies of the internal pressure effect on the transition from intrados failure to extrados failure of the cold bend are presented. The variation of PEEQ as a function of applied curvature and the internal pressure level is visualized for X60, X65 and X80. The results of X60 and X80 simulations are demonstrated after a review of our previous work with the X65 cold bend [5].

3.1 REVIEW OF THE PARAMETRIC STUDY FOR X65 COLD BEND

As it was mentioned in Section 1, PEEQ values of 40% and above are designated as an indication of material failure. Based on this failure criterion, Figure 8 shows that in case of X65 steel grade, for internal pressure values lower than 67% SMYS, PEEQ at the pipe extrados never reaches 40%. On the other hand from Figure 9 it is clear that at the same level of applied curvature the PEEQ at the intrados stays below 40% for internal pressure values greater than or equal to 67% SMYS. The graphs in Figure 8 and Figure 9 are plotted using the maximum PEEQ values at the extrados and intrados of the finite element model respectively. In the parametric studies of our previous work which resulted in Figure 8 and Figure 9, a material model with isotropic hardening was adopted. This material model assumed a linear increase of the yield stress in the plastic region of the stress-strain curve.

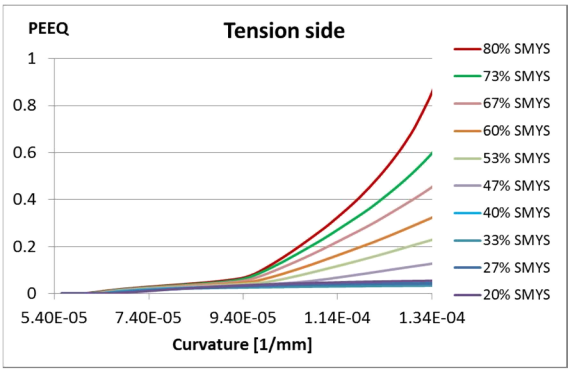

Figure 8: Variation of PEEQ (extrados) with respect to curvature for 10 different internal pressure values (X65)

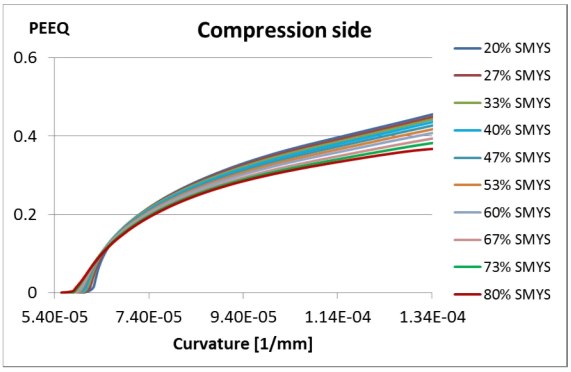

Figure 9: Variation of PEEQ (intrados) with respect to curvature for 10 different internal pressure values (X65)

In order to investigate the effect of steel grade on the distribution of PEEQ, the parametric study of internal pressure is extended to steel grades of X60 and X80, keeping the geometric configuration constant. In this way the entire range of steel grades used in the experimental study of Sen et al is simulated to investigate the effect of internal pressure on the failure mode.

3.2 ANALYSIS OF THE RELATIONSHIP BETWEEN THE TRANSITION INTERNAL PRESSURE AND CURVATURE AT FAILURE

The relationship between the curvature of the pipe axis at the point of material failure and the level of internal pressure is visualized for steel grades X60 and X80 (Figure 10).

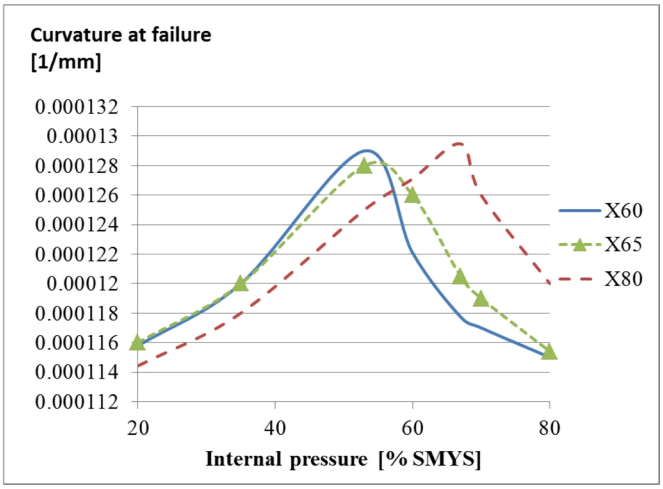

Figure 10: Variation of curvature at 40% PEEQ with respect to internal pressure

The curves in Figure 10 show the amount of applied curvature at the load stage when the maximum PEEQ in the structure reaches the value of 40%. There are several inferences that can be made using the information in Figure 10. The first inference is that all curves have peak points indicating a transition of the failure mode. For all steel grades, at the internal pressure levels on the left hand side of these peak points the material failure occurs on the compression side, whereas on the right side of the peak points the pipe failure occurs on the tension side. Because of this condition, for all steel grades a peak in the variation of the failure curvature with respect to the internal pressure indicates the transition of the failure mode from compressive to tensile. According to Figure 10 for internal pressure values less than 53% SMYS, X60 cold bends fail at the intrados, while above 53% SMYS internal pressure the failure is observed at the extrados. Furthermore, in case of X80 steel grade for internal pressure values less than 67% SMYS the failure occurs at the intrados while above this internal pressure value the failure occurs at the extrados.

The second inference from Figure 10 is that while the pipe is in the compressive failure mode, an increase in the internal pressure makes increased amounts of applied curvature necessary in order to bring the pipe to failure. This is a result of the enhanced global stiffness of the structure due to increasing internal pressure level. It is also observed that while the pipe is in the compressive failure mode the failure curvature is almost linearly proportional to the level of internal pressure except in the vicinity of the transition pressure for the case of X80 steel grade. Whereby in case of X60 steel grade the variation of the failure curvature is clearly nonlinear at both sides of the transition pressure. On the other hand while the pipe is in the tensile failure mode, less applied curvature is needed in order to cause structural failure.

It is also clear from Figure 10 that there is a shift in the transition pressure level to the right side as the steel grade increases from X60 towards X80. The peak curvature is reached by X65 steel grade at an internal pressure level of 55% SMYS which lies between the transition pressures of X60 (53% SMYS) and X80 (67% SMYS).

3.3 ANALYSIS OF THE EQUIVALENT PLASTIC STRAIN VARIATIONS AT THE COMPRESSION AND TENSION SIDES

As it is mentioned in sections 3.1 and 3.2 at certain levels of internal pressure the failure mode of the cold bend is observed to transition from compressive to tensile. Also as it is seen from Figure 10, the level of internal pressure where the transition takes place is correlated with the grade of pipe base metal. In this section the development of the PEEQ at the intrados and extrados of the cold bend are compared for internal pressure values which lie in the vicinity of the transition internal pressure. These comparisons are visualized for X60, X65 and X80 steel grades.

3.3.1 The Variation of PEEQ for X60 steel grade

In case of X60 steel grade the transition from compressive to tensile failure occurs in the vicinity of 53% SMYS internal pressure. Figure 12, Figure 13, and Figure 11 illustrate the development of the PEEQ at the intrados and extrados for 3 different levels of internal pressure in the transition zone.

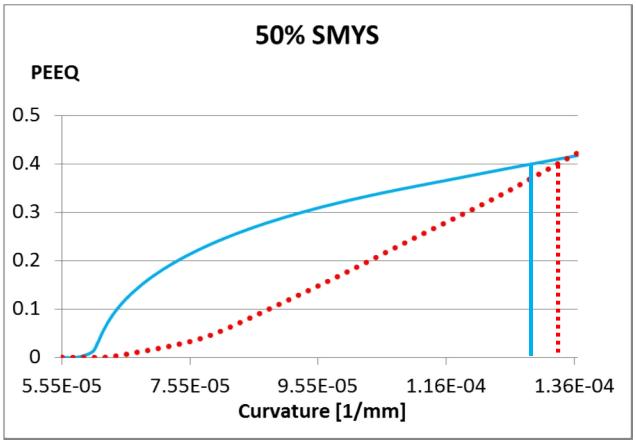

Figure 11: Compression side (solid) and tension side (dotted) variations of PEEQ (X60)

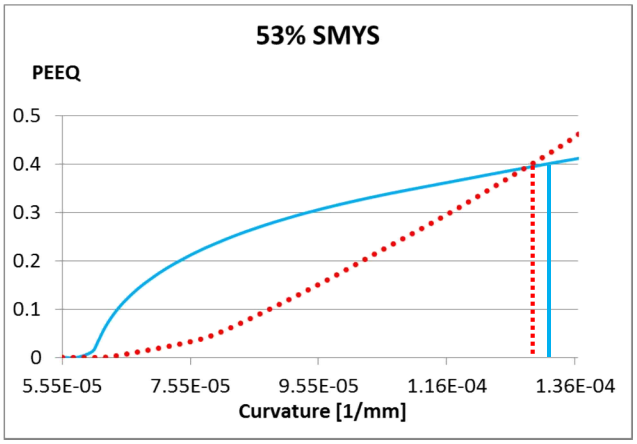

Figure 12: Compression side (solid) and tension side (dotted) variations of PEEQ (X60)

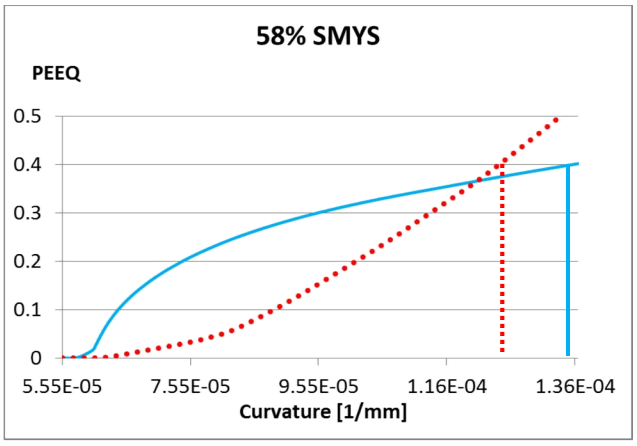

Figure 13: Compression side (solid) and tension side (dotted) variations of PEEQ (X60)

In Figure 11 for the case of 50% SMYS the intrados reaches 40% PEEQ. The straight and dotted lines perpendicular to the curvature axis mark the points at which the intrados and extrados reach 40% PEEQ respectively. From Figures 11 12, and 13, it can be observed that for 50% SMYS internal pressure the compression side fails first while for 53% and 58% the tension side fails first. The exact values of curvature at 40% PEEQ are listed for intrados and extrados, for all three internal pressure levels in Table where the critical values of curvature are highlighted in red.

Table 3: Failure curvature values for X60

Internal pressure (% SMYS)	κ at compressive failure	κ at tensile failure	$\Delta\kappa$
50	0.000129	0.000133	$-4 \cdot 10^{-6}$
53	0.000131	0.000129	$2 \cdot 10^{-6}$
58	0.000135	0.000123	$1.2 \cdot 10^{-5}$

Since the failure mode is observed to be compressive for 50% SMYS internal pressure and tensile for 53% SMYS and greater internal pressure values it is assumed that the exact transition pressure value lies between 50% SMYS and 53% SMYS for X60 steel grade. In order to estimate the exact transition pressure a linear variation of the difference between the failure curvature values of the tension and compression sides is assumed (Figure 14). In the visualization of the difference in failure curvature the minus sign in front of $\Delta\kappa$ indicates that the compression side reaches 40% PEEQ earlier than the tension side. Based on this linear variation assumption, the compressive to tensile transition pressure level can be estimated as 52% SMYS for X60 steel grade.

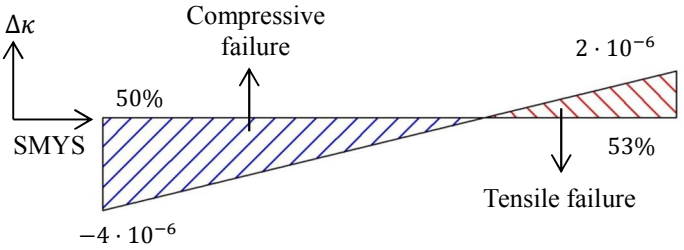

Figure 14: Variation of failure curvature difference with respect to internal pressure

3.3.2 The Variation of PEEQ for X65 steel grade

For the steel grade of X65, the transition from compressive to tensile failure is observed between 55% SMYS and 58% SMYS internal pressure. Figure 15 and Figure 16 illustrate the development of PEEQ at the intrados (solid line) and extrados (dotted line) for these two pressure levels. The vertical lines indicate 40% PEEQ for a certain applied curvature. Using the same linear approximation method of section 3.3.1, the transition pressure value for X65 cold bend is estimated as 56% SMYS.

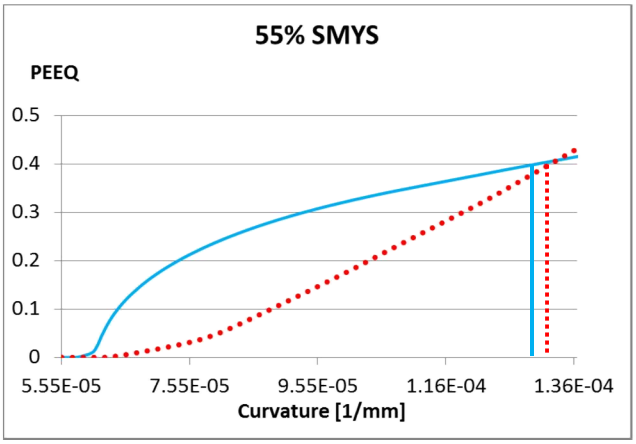

Figure 15: Compression side (solid) and tension side (dotted) variations of PEEQ (X65)

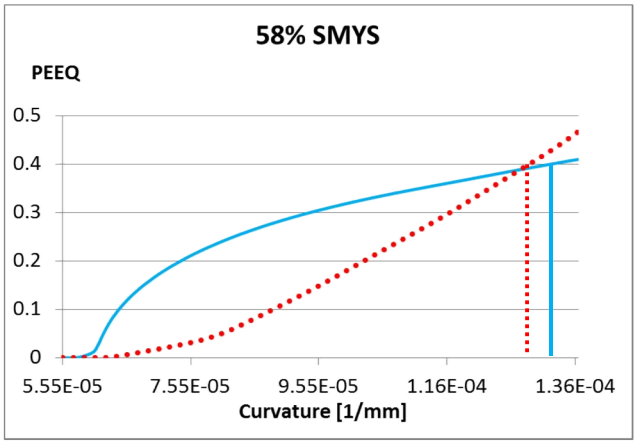

Figure 16: Compression side (solid) and tension side (dotted) variations of PEEQ (X65)

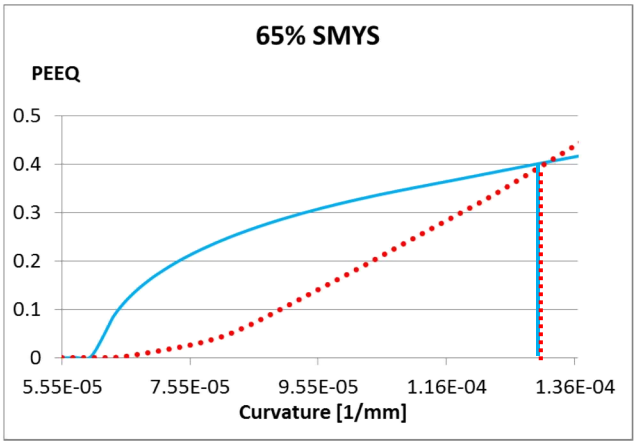

Figure 17: Compression side (solid) and tension side (dotted) variations of PEEQ (X80)

Table 2: Failure curvature values for X65

Internal pressure (% SMYS)	κ at compressive failure	κ at tensile failure	$\Delta\kappa$
55	0.0001299	0.0001318	$-1.9 \cdot 10^{-6}$
58	0.000132	0.0001284	$3.6 \cdot 10^{-6}$
60	0.000133	0.0001265	$6.5 \cdot 10^{-6}$

Table 3: Failure curvature values for X80

Internal pressure (% SMYS)	κ at compressive failure	κ at tensile failure	$\Delta\kappa$
60	0.000127	0.000138	$-1.1 \cdot 10^{-5}$
65	0.0001298	0.0001307	~0
70	0.000132	0.000126	$6 \cdot 10^{-6}$

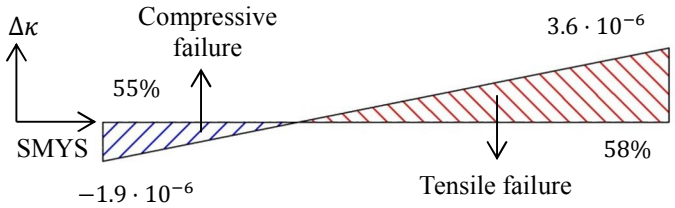

3.3.3 The Variation of PEEQ for X80 steel grade

In case of X80 steel grade the variation of PEEQ at the tension and compression sides is shown in Figure 17. According to this graph the compression and tension sides reach 40% PEEQ almost simultaneously under 65 % SMYS internal pressure. Therefore the transition internal pressure can be estimated as 65% SMYS for X80 steel grade without further approximations.

4 DISCUSSION AND SUMMARY

In the process of transporting oil and gas from its source to the location of consumption, pipelines have proven to be the most reliable method of transportation. In this process pipe direction is often changed in horizontal or vertical planes according to the variations in the terrain conditions. Changes in the pipe direction are achieved by using cold bending machines on site. In this process the mechanical properties of the pipe base metal change in such a way that the strength of the tension side increases whereas the strength of the compression side decreases. Therefore often in practice the design of cold bends for the resistance to tension side fractures is neglected due to the fact that failures are more likely to happen at the compression side of a cold bend. On the other hand, experimental studies by Sen et al and our numerical investigations of this subject revealed that there is a significant likelihood of tension side fracture in cold bends. It is also observed that the level of internal pressure determines the mode of failure to a great extent.

In this paper the effect of the internal pressure and steel grade on the failure mode of the cold bend is investigated. Parametric studies are carried out for X60, X65 and X80 steel grades which were also tested in the experimental study of Sen et al. Using finite element analysis it is verified that indeed there are two different internal pressure domains for these steel grades and the particular geometric configuration. It is found that the first of these domains consists of low pressure values

up to a certain transition pressure, whereby the second domain consists of internal pressure values higher than the transition pressure.

The pipe analyzed in this study can be considered to be a thin walled cylindrical shell structure, with stresses induced only in the axial and circumferential directions due to the applied deformation and internal pressure. At a given value for the axial deformation, the Von Mises stresses at the tension and compression sides depend on the values of both the axial and circumferential stresses. When the internal pressure is zero, the Von Mises stress on the tension side (which is the equivalent stress that causes yielding) is equal to the applied axial stress. Small values of the circumferential stresses caused by the small increments in internal pressure results in reductions of the equivalent stress values up to a certain point (Figure 18):

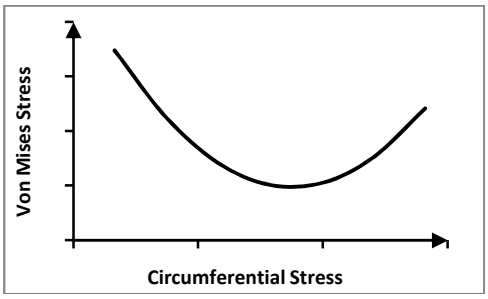

Figure 18: Variation of Von Mises Stress with increasing circumferential stress at a fixed value of tensile axial stress

On the other hand, the compression side experiences increases in the Von Mises stress values due to the increments of the circumferential stresses caused by the internal pressure. As a result, in the FEA models, the compression side buckles and then reaches the 40% PEEQ long before the tension side. For higher values of circumferential stresses, the Von Mises stresses in the tension side are higher (Figure 18). However, on the compression side, the buckle leads to a decrease in the compressive stress, and thus the tension side becomes more critical. Therefore, there exist the two distinct internal pressure domains, the boundary of which signifies the transition of the pipe failure from the compression to the tension side.

In order to determine the limits of these domains for X60, X65 and X80 cold bends, the results of the parametric studies of the internal pressure are visualized in section 3. These visualizations showed that the level of internal pressure for the transition from the compressive to the tension side failure depends on the grade of pipe steel. Also the comparison of the results of our previous parametric studies of the X65 steel grade, which assumed a linear isotropic hardening model, with the results of the current study indicates that the shape of the post-yield stress-strain curve affects the transition pressure. Furthermore it is observed that the amount of internal pressure necessary to set off the transition is linearly proportional to the strength of the steel. This linear proportionality is visualized in Figure .

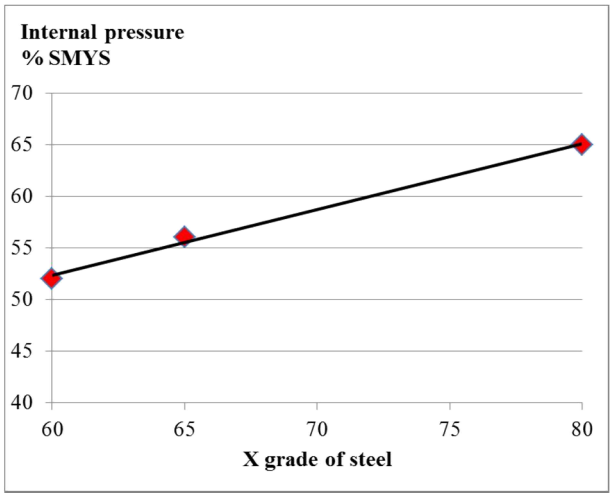

Figure 19: Relationship between the steel grade and the transition pressure

The parametric studies also provided insight into the relationship between the amount of necessary applied curvature to cause failure and the level of internal pressure. According to Figure 10 the necessary applied curvature to cause loss of containment capability increases with the level of internal pressure, as long as the pressure is within the domain of compressive failure. Whereas, if the pressure level is within the domain of tensile failure, then the necessary curvature decreases with increasing pressure.

Some of the limitations of our study include the fact that we use the same stress strain response for both the intrados and the extrados of the cold bend. We also use the same limit strain for all 3 grades. In addition, we are using an ideally curved cold bent pipe while in practice cold field bends do not have perfect curvature, but rather tend to be progressively kinked. In addition, our paper compares buckling mode and pressure for 3 pipe grades at constant D/t. Our future work will focus on investigating the effect of using more realistic stress-strain data for the intrados and extrados and different D/t ratios on the resulting transition pressure. In addition, the effect of using idealized geometry versus imperfect bends will be investigated.

Acknowledgement

Partial funding for this study was provided by NSERC

References

[1] Sen, M. (2006); “Behaviour of Cold Bend Pipes Under Combined Loads” Ph.D. dissertation, University of Alberta, 2006

[2] Sen, M., Cheng, J.J.R., Zhou, J. (2011); “Behaviour of Cold Bend Pipes under Bending Loads”
DOI: 10.1061/(ASCE)ST.1943-541X.0000219. 2011 American Society of Civil Engineers

[3] Sen, M., Cheng, J.J.R. , Murray, D. W. (2004) ; "Full-Scale Tests of Cold Bend Pipes" Proceedings of IPC2004, International Pipeline Conference, IPC2004 – 743
[4] Cakiroglu C., Komeili A., Adeeb S., Cheng, J.J.R., Sen M. (2012) ; "Numerical Analysis of High Pressure Cold Bend Pipe to Investigate the Behaviour of Tension Side Fracture", Proceedings of the 9th International Pipeline Conference, IPC2012-90381
[5] Cakiroglu C., Adeeb S., Cheng, J.J.R., Sen M. (2014); "Numerical Analysis of Pressurized Cold Bend Pipes Under Bending to Investigate the Transition from **C**ompression to Tension Side Failures", Proceedings of the Structures Congress 2014, Boston, Massachusetts
[6] Caminada S, Cumino G, Cipolla L, Di Gianfrancesco, A (2009). "Cold bending of advanced ferritic steels: ASTM grades T23, T91, T92". International Journal of Pressure Vessels and Piping 86 (2009) 853–861[7] Muraoka R., Ishikawa N., Endo S., Yoshikawa M., Suzuki N., Kondo J., Takagishi M. (2002)." Deformation and Ductile Cracking Behavior of X80 Grade Induction Bends", Proceedings of the 4th International Pipeline Conference, IPC2002-27182
[8] CSA Z662-11; Oil and gas pipeline systems - Sixth Edition; Update No. 1: January 2012, Canadian Standards Association
[9] Pressley A (2010). "Elementary Differential Geometry". ISBN: 978-1-84882-891-9, 1st edition, Springer Press